Characterization of the Metal Binding Environment of Catalytic Site 1 of Chloroplast F_1-ATPase from *Chlamydomonas*†

Wei Chen, Chia-Yuan Hu, Donald J. Crampton, and Wayne D. Frasch*

The Center for the Study of Early Events in Photosynthesis, Arizona State University, Tempe, Arizona 85287-1601

Received February 7, 2000; Revised Manuscript Received May 10, 2000

ABSTRACT: Metal ligands of the VO^{2+}−adenosine diphosphate (ADP) complex bound to high-affinity catalytic site 1 of chloroplast F_1 adenosine triphosphatase (CF_1 ATPase) were characterized by electron paramagnetic resonance (EPR) spectroscopy. This EPR spectrum contains two EPR species designated E and F not observed when VO^{2+}−nucleotide is bound to site 3 of CF_1. Site-directed mutations βE197C, βE197D, and βE197S in *Chlamydomonas* CF_1 impair ATP synthase and ATPase activity catalyzed by CF_1F_o and soluble CF_1, respectively, indicating that this residue is important for enzyme function. These mutations caused large changes in the ^{51}V hyperfine tensors of VO^{2+}−nucleotide bound to site 1 but not to site 3. Mutations to the Walker homology B aspartate βD262C, βD262H, and βD262T of *Chlamydomonas* CF_1 caused similar effects on the EPR spectrum of VO^{2+}−ADP bound to site 1. These results indicate that the conversion of the low-affinity site 3 conformation to high-affinity site 1 involves the incorporation βE197 and βD262 as metal ligands.

During ATP synthesis, the initial binding of ADP and phosphate to the F_1F_o ATP synthase triggers a conformational change in the F_1[1] portion that increases the binding affinity of the substrates at this catalytic site (*1*). In this high-affinity conformation, the equilibrium of bound substrates and products is close to unity. At an adjacent catalytic site, a conformational change also occurs that results in a decrease in the affinity of this latter site for ATP relative to ADP. In this manner, the energy from the transmembrane proton gradient is used to maintain cellular ATP concentrations in excess of that which would exist at equilibrium.

Three α and three β subunits of F_1 alternate to form a ring through which the α-helical coiled-coil of the γ subunit passes (*2, 3*). The asymmetry of the γ subunit contributes to the formation of the different conformations of the catalytic sites that are primarily located on the β subunits. The γ subunit rotates as a result of ATPase activity catalyzed by purified F_1 (*4*−*6*). Thus, during ATP synthesis, the F_o-mediated proton flux is believed to drive the rotation of the γ subunit in the opposite direction and thereby induce conformational changes of all the catalytic sites at the same time.

Nucleotides bind to the catalytic sites as a complex with Mg^{2+} that serves as a cofactor for the reaction (*7*). The metal cofactor is required for the formation of the different conformations of the catalytic sites. The conformations of each of the three catalytic sites in the crystal structure of F_1 from bovine heart mitochondria differ (*2*). One site contains Mg^{2+}-AMPPNP (β_{TP}), one has bound Mg^{2+}−ADP (β_{DP}), and one is empty (β_E). However, when crystallized with nucleotide in the absence of Mg^{2+}, the $\alpha_3\beta_3$ portion of rat liver mitochondrial F_1 shows 3-fold symmetry despite the presence of the γ subunit (*3*).

The Mg^{2+}-induced structural asymmetry of the catalytic sites also causes the large differences in nucleotide affinities (*8*). In the absence of Mg^{2+}, the three catalytic sites of *Escherichia coli* F_1 bind ATP with the same affinity. However, when ATP binds as a complex with Mg^{2+}, the affinity for nucleotides between the catalytic site conformations can differ by as much as 5 orders of magnitude. This suggests that the differences in affinity may in part result from changes in the metal ligands during the conformational changes at the catalytic sites.

Magnesium is difficult to study due to the lack of spectroscopic properties and is difficult to distinguish from water in a crystal structure. Vanadyl $(V^{IV}{=}O)^{2+}$ provides a direct probe of the types of groups that serve as ligands to the F_1 metal cofactor (*9*−*11*) because the **A** and **g** tensors derived from the EPR spectrum of the bound VO^{2+} are a direct measure of the nature of the equatorial metal ligands (*12*). The observation that site-directed mutations of a metal ligand change the ^{51}V hyperfine parameters of the EPR spectrum of F_1-bound VO^{2+} in a perceptible and predictable manner provided a means to identify specific residues as metal ligands (*13*).

Binding specificity studies of nucleotides to catalytic and noncatalytic sites on spinach chloroplast F_1 indicate that nucleotides bind to four sites that cannot be readily removed by gel filtration or dialysis. Sites 2 and 5 are noncatalytic and bind at sites primarily composed of the α subunits (*14*).

† This work was supported by National Institutes of Health Grant GM50202.

* To whom correspondence should be addressed: e-mail frasch@asu.edu; tel (480) 965-8663; fax (480) 965-6899.

[1] Abbreviations: AMPPNP, 5′-adenylyl imidodiphosphate; F_1, extrinsic membrane portion of the F_1F_o ATP synthase, CF_1, chloroplast F_1; EF_1, *Escherichia coli* F_1; MF_1, mitochondrial F_1; TF_1, thermophilic bacterial F_1; FRET, fluorescence resonance energy transfer; P-loop, phosphate-binding loop; PMS, phenazine methyl sulfate; TNP nucleotides, 2′(3′)-trinitrophenyl nucleotides; WHB, Walker homology B sequence; catch loop, mitochondrial F_1 residues βY311−319.

10.1021/bi000281n CCC: $19.00
Published on Web 07/11/2000

These sites bind ATP or 5′-adenylyl imidodiphosphate (AMPPNP) only as a complex with Mg^{2+} but will not bind ADP in the presence or absence of the cofactor. Upon isolation there exists about 1.5 mol of ADP/mol of CF_1 distributed between catalytic sites 1 and 4 (*15*). Dissociation of ADP from sites 1 and 4 is slow. However, nucleotides in the medium can exchange into these sites (*16*). Nucleotides exchange into site 4 much more slowly than at site 1 where the metal−nucleotide complex exchanges more readily than nucleotide alone (*17*). The rate of exchange at this latter site is also accelerated by the depletion of the ϵ subunit from the enzyme (*18*). Nucleotide can also bind to catalytic site 3 (*16*). Due to the lower affinity of site 3, the enzyme can be depleted of nucleotide from this site by gel filtration.

Fluorescence resonance energy transfer (FRET) measurements made with TNP nucleotides bound specifically at CF_1 sites 1−3 enabled the positions of these sites to be mapped relative to each other and to locations of fluorescent groups covalently modified at unique locations (*19*). The most extensive characterization of metal ligands by VO^{2+} EPR spectroscopy has been of CF_1 site 3 of which little is known from crystallographic methods. The ATPase activity of CF_1 is latent upon purification from F_o and the thylakoid membranes but can be activated by reduction of a disulfide on the γ subunit. In the latent form, the predominant EPR species observed when VO^{2+}−ADP complex is tightly bound to site 3 is known as species B (*10*, *11*). Under these conditions the Walker homology B (WHB) aspartate, which is βD262 in *Chlamydomonas* CF_1, was identified as a metal ligand at site 3 (*20*). The P-loop threonine (βT168 in *Chlamydomonas* CF_1) is not a metal ligand in site 3 of latent CF_1 but becomes a ligand in lieu of the Walker homology B aspartate upon activation when the EPR signal intensity from species B is converted to species C (*13*).

We now report the characterization of the EPR signal that results when VO^{2+}−ADP is bound to high-affinity catalytic site 1 of *Chlamydomonas* CF_1-ϵ. Analysis of the effects of site-directed mutations made to βD262 (the WHB aspartate) and to βE197 on this EPR spectrum indicate that these carboxyl groups coordinate the metal bound in this conformation and contribute significantly to the affinity of site 1 for the metal−ADP complex.

EXPERIMENTAL PROCEDURES

Construction of CF_1 Mutants. Strains CC-125 and CC-373 were obtained from the *Chlamydomonas reinhardtii* Culture Collection at Duke University. The template for double-stranded, oligonucleotide-mediated, site-directed mutagenesis was the pBam10.3-spec plasmid (*21*). The βD262 mutants were made as described by Hu et al. (*20*). The same protocol was used to make the βE197 mutations. The Chameleon double-stranded mutagenesis kit (Stratagene) was employed to generate *atpB* mutations on pBam10.3-spec following the provided protocol with two primers. The mutagenesis primers were as follows: βE197C, $_{5'}$GTTGGTGAACGTACCCGGTGCGGTAACGACCTTTAC$_{3'}$; βE197D, $_{5'}$GTTGGTGAACGTACCCGGGACGGTAACGACCTTTAC$_{3'}$; and βE197S, $_{5'}$GTTGGTGAACGTACCCGGTCCGGTAACGACCTTTAC$_{3'}$. The selection primer that changed the restriction site *Xmn*I to *Bam*HI was Ps, $_{5'}$CGCCCCGAAGAACGGATCCCAATGATGAGCAC$_{3'}$.

Sequences of DNA were obtained by ABI PRISM automatic sequencing to confirm the mutations in the plasmids. The sequencing primer was $_{5'}$CCGTACAGCTCCTGCTTTCG$_{3'}$. The mutated plasmids were purified by cesium chloride ultracentrifugation and diluted to 1 mg/mL prior to storage at −20 °C.

Transformation of the DNA plasmid containing mutated *atpB* genes into *C. reinhardtii* CC-373 cells employed biolistic methods using the PDS-1000 particle delivery system (Du Pont−New England Nuclear) (*21*). Southern blots with ^{32}P-labeled pBam10-spec as the probe were used as an initial screen to identify homoplasmic mutants and were confirmed by double-stranded DNA sequencing (*22*).

Biochemical Characterization of C. reinhardtii Mutants. Cell cultures were maintained for each *C. reinhardtii* strain as described by Hu et al. (*21*). The growth curves of the mutants were determined by the change in optical density (cell scattering) at 720 nm under photoautotrophic conditions (*21*). For PMS-dependent photophosphorylation measurements, the thylakoid particles were prepared according to Hu et al. (*21*). Assays were done in a 1 mL volume of reaction mixture that contained 10 μg of chlorophyll of dark-adapted thylakoid membranes, 50 mM Tricine-NaOH (pH 8.0), 10 mM NaCl, 0.2 mM $MgCl_2$, 2 mM NaH_2PO_4, 0.2 mM ADP, 2.0×10^5 cpm [α-^{32}P]ADP, 50 mM dithiothreitol, and 0.08 mM phenazine methyl sulfate. The reaction mixtures were illuminated with an Oriel-66181 lamp at 25 °C. The reactions were stopped by the addition of 4% trichloroacetic acid.

To measure ATPase activity, ammonium sulfate-precipitated CF_1 was desalted on a 1 mL centrifuge column of Sephadex G-50 in 100 mM Tricine (pH 8.0) and then stored in 20 mM tricine (pH 8.0), 10 mM KCl, 1 mM EDTA, and 5 mM ATP. ATPase activity was activated by incubating soluble CF_1 in buffer containing 50 mM dithiothreitol and 20% (v/v) ethanol for 1 h prior to assay. ATPase activity was determined by use of an ATP-regenerating system coupled to the oxidation of NADH. Each assay contained 20 mM tricine (pH 8.0), 1 mM EDTA, 50 mM dithiothreitol, 2×10^3 cpm [α-^{32}P]ATP, 11 mM $MgCl_2$, 10 mM ATP, 5 mM phospho*enol*pyruvate, 0.25 mM NADH, 8.5 units of pyruvate kinase, and 7.5 units of lactic dehydrogenase. The reactions were initiated by adding 10 μg of CF_1, followed by incubation at 37 °C. The reaction rate was based on the initial rate of change of absorption at 340 nm to measure the NADH concentration with a molar extinction coefficient of 6220, typically within the first 30 s.

Preparation of Soluble CF_1 and CF_1-ϵ. Purification of CF_1 from *Chlamydomonas* thylakoids was accomplished as per Hu et al. (*21*). The enzyme was depleted of metal-nucleotide complex from site 3 according to Chen et al. (*13*). The concentration of purified CF_1 was determined with an extinction coefficient of $\epsilon = 0.483$ cm^2 (mg of CF_1)$^{-1}$ at 277 nm (*16*).

Purification of CF_1-ϵ from *Chlamydomonas* followed the protocol used for spinach (*23*) with some modifications. The solubilized enzyme incubated for 1 h in buffer that contained 25 mM Tris-HCl (pH 7.9), 2 mM ATP, 5 mM DTT, 7.5% (v/v) glycerol, and 5% (v/v) ethanol. The protein was put on a chromatography column containing DEAE-cellulose that had equilibrated at room temperature with a buffer that contained 25 mM Tris-HCl (pH 7.9), 2 mM ATP, and 5 mM

Table 1: Functional Comparison of Wild-Type and βE197 Mutants

genotype	photoautotrophic growth rate[a] (%)	ATP synthesis activity[b] (%)	ATPase activity[c] (%)
WT	100	100	100
βE197C	6	4	3
βE197D	9	27	13
βE197S	5	10	5

[a] Measured as the rate of increase in optical density (cell scattering) of the liquid culture at 720 nm in log phase at 25 °C with a light intensity of 80 μE M^{-2} s^{-1}. [b] Based on the rate of 250 μmol of ATP (mg of chlorophyll·h)$^{-1}$ with Mg^{2+}−ADP and phosphate concentrations of 0.2 mM and 3 mM, respectively, with thylakoids from wild type. [c] Based on the rate of 9.6 μmol of ATP hydrolyzed (mg of CF_1·min)$^{-1}$ with 10 mM Mg^{2+}−ATP with CF_1 purified from wild-type *Chlamydomonas*.

dithiothreitol. After the column was washed with equilibrating buffer, the ϵ-subunit was eluted with buffer that contained 25 mM Tris-HCl (pH 7.9), 2 mM ATP, 5 mM dithiothreitol, 30% (v/v) glycerol, and 20% (v/v) ethanol. The column was washed with buffer containing 25 mM Tris-HCl (pH 7.9), and 2 mM ATP, and then CF_1-ϵ was eluted with buffer composed of 25 mM Tris-HCl (pH 7.9), 2 mM ATP, and 400 mM NaCl.

CF_1-ϵ was depleted of metal−nucleotide complex bound to site 1 by gel-filtration chromatography with Sephadex G-50 equilibrated in buffer containing 50 mM HEPES (pH 8.0), 2 mM EDTA, 1 mM ATP, and 500 mM NaCl. The fraction that contained CF_1-ϵ was concentrated to about 2 mL and then eluted from a second Sephadex G-50 column equilibrated with 50 mM HEPES (pH 8.0), 1 mM ATP, and 500 mM NaCl to remove EDTA. The sample was concentrated to 0.3 mL in 50 mM HEPES (pH 8.0) and 175 mM NaCl.

EPR Measurements. CW-EPR experiments were carried out at X-band (9 GHz) using a Bruker 580E spectrometer with a TE_{102} rectangular standard cavity and a liquid nitrogen flow cryostat operating at 125 K. Simulations of these EPR spectra were accomplished with the computer program QPOWA (*24*, *25*).

To estimate the types of groups that serve as equatorial ligands to VO^{2+} in each mutant, the observed values of $A_{||}$ derived from simulation of the EPR spectrum by QPOWA were compared with values of these tensors calculated with the coupling constants obtained from model studies (*12*, *26*) by

$$A_{||\mathrm{calc}} = \sum n_i A_{||i}/4 \qquad (1)$$

where i counts the different types of equatorial ligand donor groups, n_i(=1−4) is the number of ligands of type i, and $A_{||i}$ is the measured coupling constant for equatorial ligand donor group of type i (*12*). Similar equations were used to calculate $g_{||}$ from a given set of equatorial ligands for comparison with those derived experimentally.

RESULTS

Effects of βE197 Mutations on Catalytic Activity. The relative ability of the mutant and wild-type strains of *Chlamydomonas* to grow under photoautotrophic conditions is shown in Table 1. All of the E197 mutants affected the rate of photoautotrophic growth significantly. The initial doubling times of E197D, E197C, and E197S were about 40 h, although E197D sustained photoautotrophic growth for a longer duration than E197C and E197S.

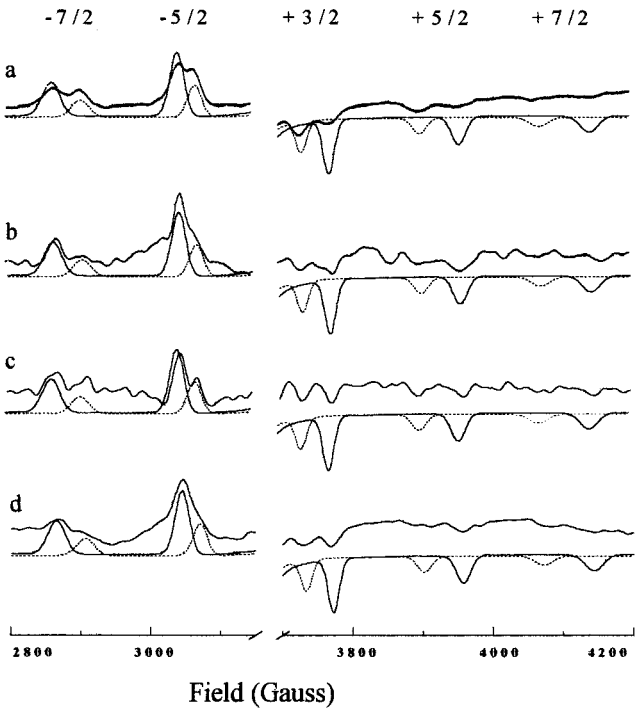

FIGURE 1: Parallel regions of VO^{2+} EPR spectra of VO^{2+}−ATP bound to site 3 of CF_1 from (**a**) wild type, (**b**) βE197C, (**c**) βE197D, and (**d**) βE197S mutants of *Chlamydomonas*. Each spectrum was obtained after addition of 1 equiv of VO^{2+}−ATP to a solution containing 60 mg of CF_1. Other EPR conditions were as follows: microwave frequency, 9.5609 GHz; number of scans, 250; field modulation frequency, 100 kHz; modulation amplitude, 0.5 mT; sweep rate, 0.95 mT/s; time constant, 82 ms; microwave power, 1.0 mW, temperature, 100 K. Simulated spectra for species B (solid lines) and species C (dotted lines) were generated by the program QPOWA with the experimental conditions above and ^{51}V hyperfine parameters from Table 2.

The rates of photophosphorylation of thylakoids isolated from the wild-type and mutant preparations are also summarized in Table 1. The rates were determined within 30 min of cell disruption where the extent of uncoupling induced by thylakoid purification was not limiting to the photophosphorylation rate (*21*). The activity of the E197D mutant, the most conservative change, was 27% that of the wild type. The activity of the other mutants was <10% of wild-type activity.

The effects of the mutations on ATPase activity of purified CF_1 were about the same as on photophosphorylation (Table 1). The highest activity was observed with the E197D mutant (13% of wild type), while E197C had the lowest activity (3%). No significant differences in the yield or subunit composition of purified CF_1 were observed between the wild type and E197 mutants.

Effects of βE197 Mutations on EPR Species from VO^{2+}−ADP Bound to site 3 of CF_1. Figure 1a shows parallel features of the EPR spectrum of VO^{2+} bound as the VO^{2+}−ATP complex to site 3 of CF_1 from wild-type *Chlamydomonas*. The types of groups coordinated at the equatorial positions of VO^{2+} strongly affect the magnitude of $g_{||}$ and $A_{||}$ that determine the position of the center of the parallel transitions and the spacing between them, respectively. Of the eight transitions that result from that fraction of VO^{2+} molecules

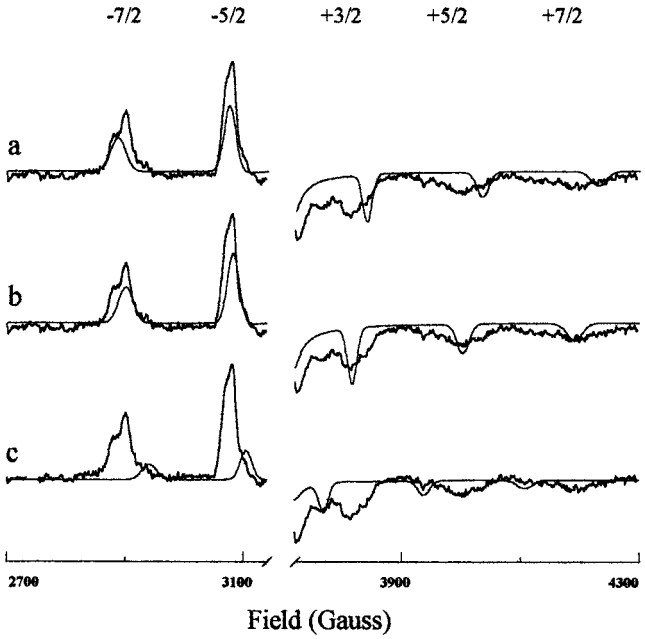

FIGURE 2: Parallel regions of VO^{2+} EPR spectra of the VO^{2+}−ADP complex bound to site 1 of CF_1-ϵ from wild-type *Chlamydomonas*. One mole equivalent of a 1:1 mole ratio of VO^{2+}−ADP was added to 38 mg of CF_1-ϵ as prepared in Experimental Procedures. EPR conditions were as follows: field modulation frequency, 100 kHz; modulation amplitude, 0.5 mT; sweep rate, 0.95 mT/s; time constant, 82 ms; microwave power, 1.0 mW, microwave frequency 9.661350 GHz, 160 scans, temperature, 125 K. Simulated spectra for species E with $A_{||} = 521$ MHz and $g_{||} = 1.9390$ (**a**), species F with $A_{||} = 501.5$ MHz and $g_{||} = 1.9455$ (**b**), and species C with $A_{||} = 456$ MHz and $g_{||} = 1.9575$ (**c**) were generated by the program QPOWA with the experimental conditions above and the ^{51}V hyperfine parameters from Table 3.

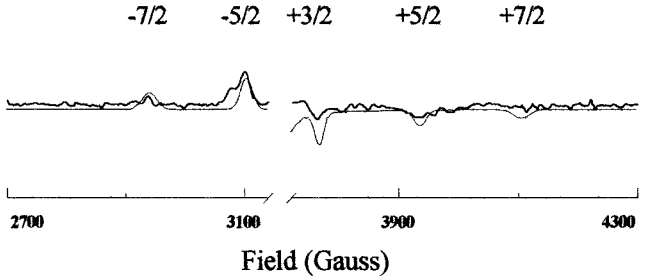

FIGURE 3: Parallel regions of VO^{2+} EPR spectra of VO^{2+}−ADP bound to CF_1-ϵ from the βE197D mutant of *Chlamydomonas*. One mole equivalent of a 1:1 mole ratio of VO^{2+}−ADP was added to 12 mg of CF_1-ϵ. EPR conditions were as follows: field modulation frequency, 100 kHz; modulation amplitude, 0.5 mT; sweep rate, 0.95 mT/s; time constant, 82 ms; microwave power, 1.0 mW; temperature, 125 K; field modulation frequency, 9.65741 GHz; number of scans, 808. The simulated spectrum (dotted line) was generated from the ^{51}V hyperfine parameters in Table 3.

where the molecular axis (defined by the oxo bond) is aligned parallel with the magnetic field, the $-^{7}/_{2||}$, $-^{5}/_{2||}$, $+^{3}/_{2||}$, $+^{5}/_{2||}$, and $+^{7}/_{2||}$ transitions (shown) do not overlap with the perpendicular transitions.

Two sets of parallel transitions are observed in Figure 3 from VO^{2+}−ATP bound to latent site 3 that correspond to EPR species B and C as reported previously (*13*). The simulated spectra for EPR species B and C (continuous and dotted lines, respectively) were derived from the values of $A_{||}$ and $g_{||}$ shown in Table 2. The parallel transitions of the EPR spectra from VO^{2+}−ATP bound to site 3 of the E197C, E197D, and E197S mutants of CF_1 are shown in Figure 1, spectra b, c, and d, respectively. Simulation of these spectra resulted in the same values of $A_{||}$ and $g_{||}$ that were observed with the wild-type enzyme (Table 2). Thus, E197 is not an equatorial ligand to VO^{2+} at site 3 in the conformations that give rise to either species B or species C.

Table 2: ^{51}V Hyperfine Tensors of EPR Species Observed from Vanadyl Bound as VO^{2+}−ATP to site 3 of Wild-Type and βE197 Mutants of CF_1

	species B[a]		species C[a]	
genotype	$A_{||}$ (MHz)	$g_{||}$	$A_{||}$ (MHz)	$g_{||}$
wild type	497.5	1.9475	456.5	1.9575
E197C	497.5	1.9475	456.5	1.9575
E197D	497.5	1.9475	456.5	1.9575
E197S	497.5	1.9475	456.5	1.9575

[a] Derived by simulation of the experimental spectra with QPOWA.

Characterization of EPR species from VO^{2+}−ADP Bound to CF_1-ϵ. Addition of 1 equiv of VO^{2+}−ADP to wild-type CF_1-ϵ prepared as described in Experimental Procedures resulted in the EPR spectrum shown in Figure 2. Under these conditions, the metal−ADP complex preferentially binds to site 1 of the enzyme (*18*). Three EPR species were observed. The simulated spectra that provide the best fit to each species are also shown in Figure 2. These spectra were obtained under the experimental conditions with the values for $A_{||}$ and $g_{||}$ shown in Table 3.

The majority of the signal intensity (54%) derived from VO^{2+}−ADP bound to site 1 in a manner that gave rise to an EPR species designated species F for which the value of $A_{||}$ was 501.5 MHz. On the basis of $A_{||}$ alone, it appears that this species might be similar to EPR species B observed when VO^{2+}−nucleotide is bound to site 3 of latent CF_1. However, the simulated spectrum of EPR species B, based on the ^{51}V hyperfine couplings in Table 2, is not a good fit to this spectrum due to differences in $g_{||}$. Thus, EPR species F results from VO^{2+} bound in a manner that differs from that which gives rise to EPR species B. An EPR species designated species E for which the value of $A_{||}$ was 521 MHz accounted for 36% of the signal intensity. The remaining 10% of the EPR signal intensity resulted from a species with ^{51}V-hyperfine tensors closely similar to EPR species C that originates from VO^{2+}−nucleotide bound to site 3.

The best fit of EPR species E to eq 1 is consistent with three equatorial oxygen ligands from carboxyl or phosphate groups and one equatorial oxygen ligand from a water molecule. The equatorial ligands that fit best with EPR species F to eq 1 differ from species E only in that a hydroxyl oxygen from a tyrosine is the fourth ligand in lieu of the water. The residue analogous to *Chlamydomonas* $CF_1\beta$E197 is within 5 Å of the Mg^{2+} at the β_{DP} site of bovine MF_1 as is the Walker homology B aspartate (βD262 in *Chlamydomonas*) (*2*). The effects of mutations to these residues on the binding of VO^{2+}−ADP to site 1 of CF_1-ϵ were examined for changes in the ^{51}V hyperfine tensors as an indication of metal coordination.

Effects of βE197 Mutations on EPR Species from VO^{2+}−ADP Bound to CF_1-ϵ. Figure 3 shows parallel transitions of EPR spectra of VO^{2+} bound as VO^{2+}−ADP to CF_1-ϵ containing the βE197D mutation. The total intensity of the EPR signal is directly proportional to the amount of VO^{2+} bound to the enzyme (*13*). The signal intensity per mole of

Table 3: ^{51}V Hyperfine Tensors of EPR Species Observed from Vanadyl Bound as VO^{2+}−ADP to Wild-Type and Mutant CF_1-ϵ

genotype	total signal intensity[a] (% of wild type)	$A_{\|\|}$[b] (MHz)	$g_{\|\|}$[b]	signal intensity of each EPR species[c] (% of wild type)	
wild type	100	456.5	1.9575	10 ± 2	species C
		501.5	1.9455	54 ± 4	species F
		521.0	1.9390	36 ± 5	species E
βE197D	16	456.5	1.9575	16 ± 2	
βE197C	41	457.5	1.9575	10 ± 2	
		497.5	1.9475	31 ± 2	
βE197S	41	456.5	1.9575	9 ± 1	
		497.5	1.9475	32 ± 3	
βD262H	56	456.5	1.9580	25 ± 1	
		498.0	1.9475	31 ± 1	
βD262T	51	458.0	1.9575	26 ± 1	
		496.5	1.9475	26 ± 1	
βD262C	46	457.5	1.9575	9 ± 1	
		497.5	1.9465	14 ± 2	
		529.5	1.9370	23 ± 2	

[a] Calculated as intensity (mole of CF_1-ϵ·scan)$^{-1}$. [b] Derived from the simulation of the EPR spectrum with QPOWA. [c] Calculated as intensity (mole of CF_1-ϵ·scan)$^{-1}$ as a percentage of the total signal intensity of wild type.

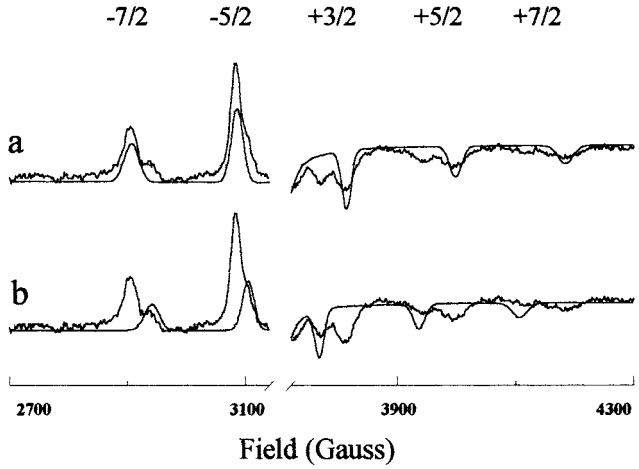

FIGURE 4: Parallel regions of VO^{2+}-EPR spectra of VO^{2+}−ADP bound to CF_1-ϵ from the βE197C mutant of *Chlamydomonas*. One mole equivalent of a 1:1 mole ratio of VO^{2+}−ADP was added to 25 mg of CF_1-ϵ. EPR conditions were as follows: field modulation frequency, 100 kHz; modulation amplitude, 0.5 mT; sweep rate, 0.95 mT/s; time constant, 82 ms; microwave power, 1.0 mW; temperature, 125 K; field modulation frequency, 9.663416 GHz; number of scans, 360. Simulated spectra obtained from the EPR conditions above with $A_{\|}$ = 497.5 MHz and $g_{\|}$ = 1.9475 (**a**) or with $A_{\|}$ = 456.5 MHz and $g_{\|}$ = 1.9575 (**b**) were generated as in Figure 2.

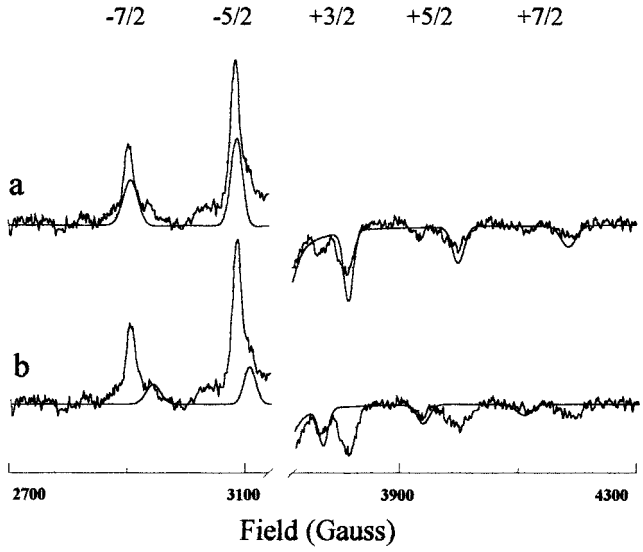

FIGURE 5: Parallel regions of VO^{2+} EPR spectra of VO^{2+}−ADP bound to CF_1-ϵ from the βE197S mutant of *Chlamydomonas*. One mole equivalent of a 1:1 mole ratio of VO^{2+}−ADP was added to 18 mg of CF_1-ϵ. EPR conditions were as follows: field modulation frequency, 100 kHz; modulation amplitude, 0.5 mT; sweep rate, 0.95 mT/s; time constant, 82 ms; microwave power, 1.0 mW; temperature, 125 K; field modulation frequency, 9.66169 GHz; number of scans, 362. Simulated spectra obtained from the EPR conditions above with $A_{\|}$ = 497.5 MHz and $g_{\|}$ = 1.9475 (**a**) or with $A_{\|}$ = 456.5 MHz and $g_{\|}$ = 1.9575 (**b**) were generated as in Figure 2.

enzyme per scan of the E197D mutant was only 16% that of the wild type (Table 3). Thus, compared to the wild-type enzyme, very little binding of VO^{2+}−ADP occurred. A single EPR species was observed for which the ^{51}V-hyperfine coupling was closely similar to EPR species C of site 3 (Table 3).

The E197C and E197S mutations affected the binding of VO^{2+}−ADP to site 1 of CF_1-ϵ in a similar manner (Figures 4 and 5). The signal intensity per mole of enzyme per scan of these mutants was about half (41%) that observed with wild type. Neither EPR species E or F was observed with these mutants. Instead, the majority of the signal intensity in the spectra of the E197C and E197S mutants derived from an EPR species for which $A_{\|}$ was 497.5 MHz. The ^{51}V hyperfine tensors of this species are closely similar to those of EPR species B of site 3. The equatorial ligands for this species that fit eq 1 best consist of two oxygens from carboxyl or phosphate groups, a hydroxyl oxygen from serine or threonine, and a water molecule. The EPR species comparable to species C of site 3 ($A_{\|}$ = 456 MHz) was still present. On the basis of the signal intensity per mole of enzyme per scan, the signal intensity of this species in both mutants was about the same (10%) as observed in the wild type.

Effects of βD262 Mutations on EPR Species from VO^{2+}−ADP Bound to CF_1-ϵ. The EPR spectra from VO^{2+}−ADP bound to site 1 of CF_1-ϵ that contain the WHB aspartate mutations βD262H and βD262T are shown in Figures 6 and 7, respectively. The effects of these mutations on the EPR spectra were similar to those of the E197C and E197S mutations. The total signal intensity per mole of enzyme per

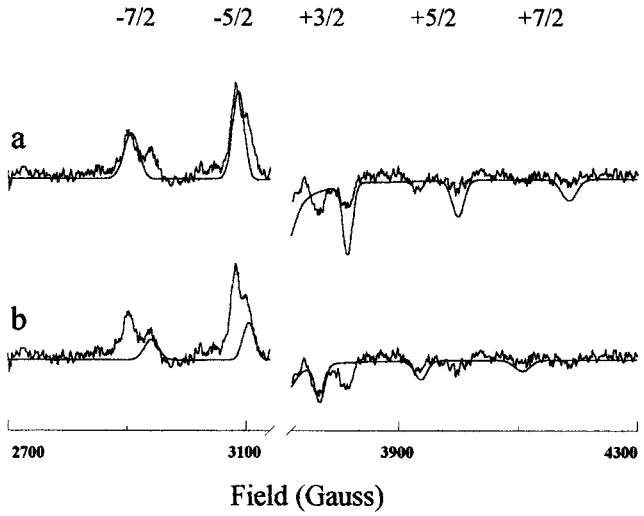

FIGURE 6: Parallel regions of VO^{2+} EPR spectra of VO^{2+}−ADP bound to CF_1-ϵ from the βD262H mutant of *Chlamydomonas.* One mole equivalent of a 1:1 mole ratio of VO^{2+}−ADP was added to 15 mg of CF_1-ϵ. EPR conditions were as follows: field modulation frequency, 100 kHz; modulation amplitude, 0.5 mT; sweep rate, 0.95 mT/s; time constant, 82 ms; microwave power, 1.0 mW; temperature, 125 K; field modulation frequency, 9.66251 GHz; number of scans, 180. Simulated spectra obtained from the EPR conditions above with $A_{||}$ = 497.5 MHz and $g_{||}$ = 1.9475 (**a**) or with $A_{||}$ = 456.5 MHz and $g_{||}$ = 1.9575 (**b**) were generated as in Figure 2.

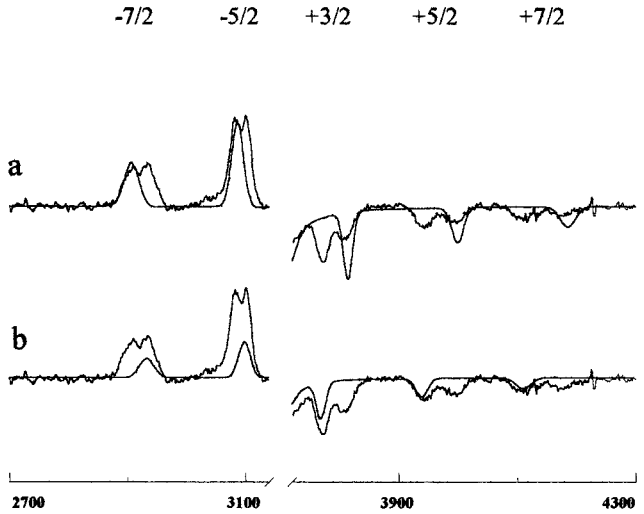

FIGURE 7: Parallel regions of VO^{2+} EPR spectra of VO^{2+}−ADP bound to CF_1-ϵ from the βD262T mutant of *Chlamydomonas.* One mole equivalent of a 1:1 mole ratio of VO^{2+}−ADP was added to 15 mg of CF_1-ϵ. EPR conditions were as follows: field modulation frequency, 100 kHz; modulation amplitude, 0.5 mT; sweep rate, 0.95 mT/s; time constant, 82 ms; microwave power, 1.0 mW; temperature, 125 K; field modulation frequency, 9.662505 GHz; number of scans, 400. Simulated spectra obtained from the EPR conditions above with $A_{||}$ = 497.5 MHz and $g_{||}$ = 1.9475 (**a**) or with $A_{||}$ = 456.5 MHz and $g_{||}$ = 1.9575 (**b**) were generated as in Figure 2.

scan of the D262H and D262T mutants was 10−15% higher (56% and 51%, respectively) than in the E197C and E197S mutants (Table 3). These small increases in total intensity were due to an increase in the amount of the signal intensity comparable to species C of site 3 ($A_{||}$ = 456 MHz). As with the other mutants, an EPR species with ^{51}V hyperfine tensors

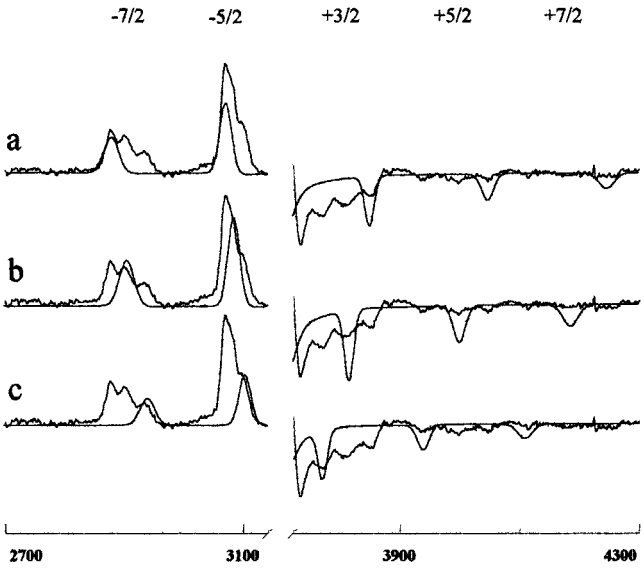

FIGURE 8: Parallel regions of VO^{2+} EPR spectra of VO^{2+}−ADP bound to CF_1-ϵ from the βD262C mutant of *Chlamydomonas.* One mole equivalent of a 1:1 mole ratio of VO^{2+}−ADP was added to 27 mg of CF_1-ϵ. EPR conditions were as follows: field modulation frequency, 100 kHz; modulation amplitude, 0.5 mT; sweep rate, 0.95 mT/s; time constant, 82 ms; microwave power, 1.0 mW; temperature, 125 K; field modulation frequency, 9.659345 GHz; number of scans, 425. Simulated spectra obtained from the EPR conditions above with $A_{||}$ = 529 MHz and $g_{||}$ = 1.9370 (**a**), with $A_{||}$ = 497.5 MHz and $g_{||}$ = 1.9475 (**b**), and with $A_{||}$ = 456.5 MHz and $g_{||}$ = 1.9575 (**c**) were generated as in Figure 2.

similar to species B of site 3 ($A_{||}$ was 498 MHz) was observed. The signal intensity of this species was comparable to that observed in CF_1-ϵ that contained the E197C and E197S mutants.

Figure 8 shows parallel transitions of EPR spectra of VO^{2+} bound as VO^{2+}−ADP to CF_1-ϵ containing the βD262C mutation. As with the other mutants, the affinity of VO^{2+}−ADP for site 1 was decreased by about 2-fold from wild-type CF_1-ϵ (to 46% of wild type, Table 3) and EPR species E and F were not observed. The EPR species with $A_{||}$ of 456 MHz (equivalent to species C) was present with the same relative signal intensity (9%) as in the wild type (Figure 8c). Although the EPR species similar to species B of site 3 was observed, its signal intensity was about half (14%) of that observed in CF_1-ϵ that contained the other mutants examined (Figure 8b). An EPR species with $A_{||}$ = 529 MHz comprised the majority of the signal intensity (23%) observed in CF_1-ϵ that contained the D262C mutation (Figure 8a). The equatorial ligands for this species that fit best to eq 1 consist of two oxygens from carboxyl or phosphate and two oxygens from water molecules. Thus, this species differs from species E by a single substitution of a carboxyl for a water molecule.

DISCUSSION

The results presented here describe the binding environment of the metal−ADP complex at the high-affinity catalytic site 1 of CF_1-ϵ that is clearly distinct from that found at the low affinity catalytic site 3. The data indicate that both E197 and D262 contribute ligands to the metal cofactor only in the high-affinity conformation of the activated enzyme.

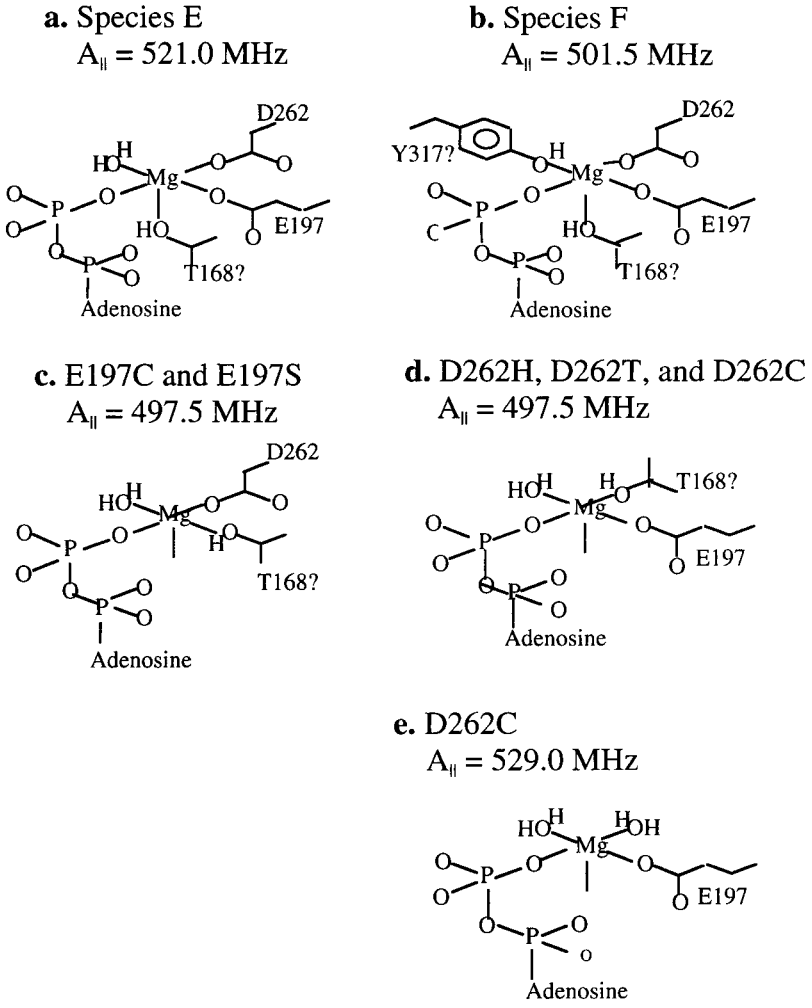

FIGURE 9: Summary of effects of mutations on the metal coordination of VO^{2+}−ADP bound to site 1 of CF_1-ϵ. The types of groups shown as equatorial ligands were derived from best fits of the ^{51}V hyperfine values from Table 3 to eq 1.

The Mg^{2+} cofactor is required to induce the catalytic site conformations that differ in their affinity for nucleotide (*8*). Thus, the conformational changes that promote the selective release of ATP from the enzyme result in part from changes in the coordination of the metal.

The ^{51}V hyperfine tensors of VO^{2+}−nucleotide bound to the EPR species C form of site 3 was not affected by either the mutations to E197 (Figure 1) or to D262 (*20*), indicating that neither residue was an equatorial VO^{2+} ligand in this conformation. Of the three EPR species observed upon addition of 1 equiv of VO^{2+}−ADP to site 1 of CF_1-ϵ, the species closely similar to the activated form of site 3 (species C) comprised about 10% of the bound VO^{2+}−ADP. Neither the E197 or D262 mutations altered the abundance or ^{51}V hyperfine parameters of this species significantly. Thus, about 10% of the VO^{2+}−ADP probably became bound to site 3 of CF_1-ϵ. Since depletion of the ϵ subunit activates the enzyme, EPR species B, observed when VO^{2+}−nucleotide is bound to site 3 of latent CF_1 (Figure 1), is not anticipated to be present under the conditions in which VO^{2+}−ADP is bound to site 1 of CF_1-ϵ.

Under the conditions in which VO^{2+}−ADP is bound to site 1 of CF_1-ϵ presented here, the metal−nucleotide complex can exist in either of two conformations that give rise to EPR species E and F. All of the mutations to E197 and D262 examined affected these EPR species indicating that the carboxyl groups from both residues serve as equatorial metal ligands. In most of the mutants, addition of VO^{2+}−ADP to CF_1-ϵ resulted in the formation of an EPR species that closely resembles EPR species B from VO^{2+}−nucleotide bound to site 3 of latent CF_1. However, it is unlikely that this EPR species results from VO^{2+}−ADP bound to site 3 in the species B conformation for two reasons. First, activation of the enzyme converts the VO^{2+}−ADP bound to site 3 from the species B to the species C form (*10*, *11*). Second, the D262 mutations have been shown to change the ^{51}V hyperfine parameters of species B from VO^{2+}−nucleotide bound to site 3 (*20*). However, niether the value of $A_{||}$ nor $g_{||}$ from the "species B-like" signal of VO^{2+}−ADP bound to site 1 was affected by these same mutants (Table 3). Thus, it is unlikely that the mutations created a condition in which the metal−ADP complex bound to the latent form of site 3 preferentially to site 1.

Figure 9 shows a summary of the most probable equatorial ligands in each mutant based on the types of groups that best fit as equatorial ligands calculated from eq 1 with the values of $A_{||}$ and $g_{||}$ from Table 3. The presence of this EPR species with $A_{||}$ = 498 MHz (similar to species B) when VO^{2+}−ADP is bound to site 1 of the E197 and D262 mutants is explained by a hydroxyl ligand from a serine or threonine in lieu of the carboxyl group that was mutated. With the E197C and E197S mutants, the carboxyl of D262 remains a

ligand (Figure 9c), while the D262H, D262T, and D262C mutants retain the carboxyl of E197 as a ligand (Figure 9d). The **A** and **g** tensors that result are the same in either case. Although the identity of the hydroxyl group is unknown, the P-loop threonine is the most likely candidate (*2*, *13*).

For that fraction of the wild-type enzyme in which the bound VO^{2+}−ADP gave rise to EPR species E, the ligands of Figure 9c,d represent a single ligand substitution as the result of the mutations. In the remaining fraction that gave rise to species F, this substitution was accompanied by a second in which a tyrosine hydroxyl was replaced by a water ligand. Although the identity of the tyrosine is unknown, the catch-loop tyrosine (βY317 in *Chlamydomonas* CF_1) is a likely candidate. An additional EPR species was also observed in the D262C mutant ($A_{||} = 529$ MHz). As shown in Figure 9e, a water molecule has substituted for the carboxyl group in a substantial fraction of the sample.

The most conservative mutation examined was E197D, which retains a carboxyl group but has a shorter side chain. From the data of Figure 3, it appears that this mutation decreased the affinity of site 1 for the VO^{2+}−ADP such that the addition of a single equivalent of the metal−nucleotide only resulted in the residual binding to site 3 (species C). This mutation had the highest activity of all the mutants examined. A possible reason is that E197D does not promote the formation of incorrect conformations of the metal−ADP complex tightly bound to site 1 (Figure 9c−e) that would interfere with activity.

The entrapment of Mg^{2+}−ADP in a nonfunctional conformation at a high-affinity site inhibits the ATPase activity of soluble F_1 ATPases (*27*). The partition of the VO^{2+}−ADP bound at site 1 into conformations that give rise to either EPR species E or F may represent the functional and nonfunctional (entrapped) conformations of the metal−ADP complex. Recent evidence suggests that the binding of Mg^{2+}−ADP to high-affinity catalytic sites 1 and 4 can inhibit Mg^{2+}-ATPase activity and that the binding of Mg^{2+} to low-affinity sites 3 and 6 can slow the rate of hydrolysis further (*28*).

According to the binding change mechanism (*1*), a conformational change triggered by the binding of substrates to the empty site increases the substrate affinity at that site. In this high-affinity conformation, the equilibrium of bound substrates and products is close to unity. The catalytic cycle at this site is completed by subsequent conformational changes that return the site to the low-affinity form. Dissociation of ATP can then occur even against an unfavorable chemical gradient because this conformation of the site has lower affinity for ATP relative to ADP.

In the absence of Mg^{2+}, the different conformations of the site actually have the same affinity for nucleotide (*8*). The requirement for the Mg^{2+}−nucleotide complex to induce the differences in affinities between enzyme conformations implies that the metal contributes significantly to the juxtaposition of the nucleotide to residues in the catalytic site. In the conformation with low affinity (site 3), the metal ligands are primarily hydroxyl groups (*13*). Metal coordination by the carboxyl groups of E197 and D262 in high-affinity site 1 reported here indicates that the conformational change of the site causes changes in the metal ligands. Carboxyl groups coordinate hard metals such as Mg^{2+} with higher affinity than do hydroxyl groups that coordinate the metal at site 3 (*13*). Due to this difference in affinity, metal coordination by E197 and D262 may be sufficient to pull the Mg^{2+}−nucleotide complex into a position that results in the juxtaposition of nucleotide with residues such as the P-loop lysine that result in the overall dissociation constant for nucleotide and facilitate ATP synthesis.

REFERENCES

1. O'Neal, C. C., and Boyer, P. D. (1984) *J. Biol. Chem. 259*, 5761−5767.
2. Abrahams, J. P., Leslie, G. W., Lutter, R., and Walker, J. E. (1994) *Nature 370*, 621−628.
3. Bianchet, M. A., Hullihen, J., Pedersen, P. L., and Amzel, L. M. (1998) *Proc. Natl. Acad. Sci. U.S.A. 95*, 11065−11070.
4. Duncan, T. M., Bulygin, V. V., Zhou, Y., Hutcheon, M. L., and Cross, R. L. (1995) *Proc. Natl. Acad. Sci. U.S.A. 92*, 10964−10968.
5. Sabbert, D., Engelbrecht, S., and Junge, W. (1996) *Nature 381*, 623−626.
6. Noji, H., Yasuda, R., Yoshida, M., and Kinosita, K., Jr. (1997) *Nature 386*, 299−302.
7. Frasch, W. D., and Selman, B. R. (1982) *Biochemistry 21*, 3636−3643.
8. Weber, J., Bowman, C., and Senior, A. E. (1996) *J. Biol. Chem. 271*, 18711−18718.
9. Houseman, A. L. P., LoBrutto, R., and Frasch, W. D. (1994) *Biochemistry 33*, 4910−4917.
10. Houseman, A. L., LoBrutto, R., and Frasch, W. D. (1994) *Biochemistry 33*, 10000−10006.
11. Houseman, A. L., LoBrutto, R., and Frasch, W. D. (1995) *Biochemistry 34*, 3277−3285.
12. Chasteen, N. D. (1981) in *Biological Magnetic Resonance* (Berliner, L. and Reuben, J., Eds.) pp 53−119, Plenum Press, New York.
13. Chen, W., LoBrutto, R., and Frasch, W. D. (1999) *J. Biol. Chem 274*, 7089−7094.
14. Shapiro, A. B, and McCarty, R. E. (1990) *J. Biol. Chem. 265*, 4340−4347.
15. Digel, J. G., and McCarty, R. E. (1995) *Biochemistry 34*, 14482−14489.
16. Bruist, M. F., and Hammes, G. G. (1981) *Biochemistry 20*, 6298−9305.
17. Digel, J. G., Kishinevshy, A., Ong, A. M., and McCarty, R. E. (1996) *J. Biol. Chem. 269*, 19976−19982.
18. Sotoropolous, P., Ong, A. M., and McCarty, R. E. (1994) *J. Biol. Chem. 269*, 19810−19816.
19. McCarty, R. E., and Hammes, G. G. (1987) *Trends Biochem. Sci. 12*, 234−237.
20. Hu, C.-W., Chen, W., and Frasch, W. D. (1999) *J. Biol. Chem. 274*, 30481−30486
21. Hu, C.-Y., Houseman, A. L. P., Morgan, L., Webber, A. N., and Frasch, W. D. (1996) *Biochemistry 35*, 12201−12211.
22. Sambrook, J., Fritsch, E. F., and Maniatis, T. (1989) in *Molecular Cloning, A Laboratory Manual*, p 9.31−9.55, Cold Spring Harbor Laboratory Press, Cold Spring Harbor, NY.
23. Richter, M., Patrie, W. J., and McCarty, R. E. (1984) *J. Biol. Chem. 259*, 7371−7373.
24. Nilges, M. J. (1979) Electron Paramagnetic Resonance Studies of Low Symmetry Nickel (I) and Molybenum (V) Complexes, Ph.D. Thesis, University of Illinois, Urbana, IL.
25. Maurice, A. M. (1980) Acquisition of Anisotropic Information by Computational Analysis of Isotropic EPR Spectra, Ph.D. Thesis, University of Illinois, Urbana, IL.
26. Hamstra, B. J., Houseman, A. L., Colpas, G. J., Kampf, J. W., LoBrutto, R., Frasch, W. D., and Pecoraro, V. L. (1997) *Inorg. Chem. 36*, 4866−4874.
27. Drobinshaya, I. Y., Kozlov, I. A., Murataliev, M. B., and Vulfson, E. N. (1985) *FEBS Lett. 182*, 419−424.
28. Digel, J. G., Moore, N. D., and McCarty, R. E. (1998) *Biochemistry 37*, 17209−17215.

BI000281N